CHAPTER 14

A MAMMOGRAPHIC REGISTRATION FRAMEWORK BASED ON ANATOMICAL LINEAR STRUCTURES

Robert Martí
University of Girona, Spain

Caroline M. E. Rubin
Royal South Hants Hospital, UK

Erika R. E. Denton
Norfolk and Norwich University Hospital, UK

Reyer Zwiggelaar
University of Wales, UK

CONTENTS

14.1 INTRODUCTION

Various registration approaches have been adopted to correlate areas in mammograms and detect differences. These differences are likely to be associated with the development of an abnormality. Most of these methods rely on corresponding landmarks between images. Obtaining these landmarks turns out to be the most difficult task and plays an important role in the alignment accuracy. Manual landmark generation is a tedious and time-consuming task when the number of landmarks is large and, moreover, introduces variability in placing the landmarks (two consecutive experiments with the same images could have different landmarks and errors). Therefore, a large number of these methods are based on automatically extracting and corresponding landmarks from mammographic images. The landmarks include breast boundary,[1–3] pectoral muscle,[3] salient regions extracted using wavelets,[4] isointensity contours[5] or steerable filters,[2] and crossing points of horizontal and vertical structures.[6]

This chapter presents an approach to extract correspondence in mammographic images based on anatomical features that appear as linear structures (i.e., fibrous tissue, ducts, and vessels). Correspondence is used here in two different applications: for mammographic image registration and for tracking linear structures.

Registration is applied to temporal and contralateral mammograms of the same woman. A framework for the detection of abnormal structures based on registration is developed, and some initial promising results are given. Tracking of linear structures (see Section 14.6) is performed for the same breast over several screening rounds. This could be used to assess and model the development of architectural changes and abnormal structures. By being able to track regions back in time, the available information helps to improve early detection of subtle abnormalities that are initially missed by radiologists. One could argue that contralateral registration based on the linear structures in the left and right breasts should not be performed because linear structures present large differences. However, it is generally accepted that overall duct, vessel, and tissue structure shows similarities between left and right breasts of the same woman. Figure 14.1 illustrates those similarities in temporal and contralateral images. The aim is to use these similarities to guide the registration process.

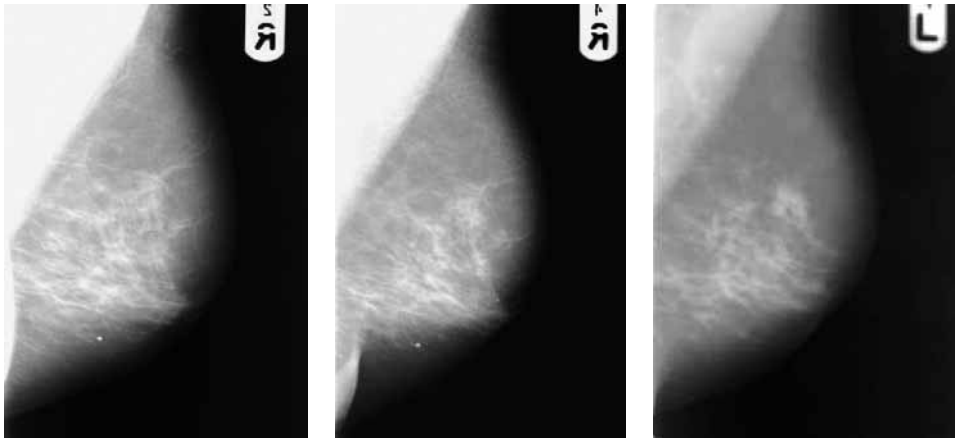

(a) (b) (c)

Figure 14.1 Similarities between temporal and contralateral mammograms: (a) right breast obtained in 1992; (b) right breast obtained in 1995; and (c) left breast obtained in 1995.

14.2 CORRESPONDENCE OF MAMMOGRAPHIC IMAGES

Many scientific subject areas (i.e., medicine, remote sensing) have to deal with the problem of image correspondence (also known as image registration or image matching). This problem arises when there is a need to extract information about an object by comparing a set of different images in which this object appears. Most of the time, this comparison cannot be performed easily because of differences between images such as viewpoint changes, use of different sensors, images taken at different times, and changes in general imaging conditions. Given such differences, a way to align different images of the same object is needed. In medical applications, and specifically in mammography, radiologists have to deal with all the above problems. For example, a way to detect abnormal structures in the breast is to compare temporal (images of the same breast taken at different times) or contralateral (using left-right breast) mammograms.

Since images are taken under different conditions (i.e., film sensitivity, radiation exposure, breast compression, and patient movement) and/or time intervals (e.g., screening interval of three years), the structure of the breast is likely to suffer some changes, although overall similarity will be maintained. A way to detect those changes is to align the images and compare the results using, for instance, simple image subtraction.

A general methodology for image alignment typically follows these steps:

(1) *Selection and extraction of features.* A registration method can be based on matching different image primitives. For instance: points,[7] edges,[8] ridges,[9,10] surfaces,[11] or a whole image.[12–15] The selection of a suitable

primitive is a trade-off between the information it provides and its complexity. For instance, raw pixels with only intensity information provide a straightforward comparison. On the other hand, taking the whole image provides more (and more complex) information. Primitives are described by a set of features extracted from them. This is the case, for instance, for shape features extracted from regions or curvature values extracted from linear structures.

(2) *Similarity metric.* A way to measure the similarity between the extracted features is needed. Many different similarity metrics have been proposed and their suitability depends on the chosen feature.

(3) *Selection of the mapping function and estimation of its parameters.* The complexity of a mapping function should be determined depending on the application field and type of misalignment being dealt with. Once a mapping function is selected, its parameters need to be estimated. This requires a definition of an optimum search space and search strategy that is often related to cost function optimization, which is related to a similarity measure previously mentioned.

(4) *Alignment of images using the mapping function.* When the function parameters are known, an image can be transormed in order to minimize the initial misalignment.

The remainder of this section presents various image-registration approaches. Methods investigated are split into point-based and mutual-information-based approaches. In addition, a hybrid approach is proposed, which incorporates aspects from point- and correlation-based methods. Algorithms and initial results are given for both x-ray and MR images. In addition, x-ray registration are further evaluated using a larger data set to determine a suitable transformation function.

X-ray registration is performed using temporal mammograms—mammograms of the same breast and same woman taken three years apart. A pair of temporal mammograms and the difference image (where darker areas indicate larger misregistration) are shown in Fig. 14.2. It is clear that there are large differences near the pectoral muscle and the breast edge; but also, internally there are significant mismatched areas.

Three-dimensional registration of MR images has generally been applied to dynamic sequences registering a precontrast volume to a volume after a contrast agent had been injected. In this case, misalignment is usually small, generally due to patient movement, and intensity distribution in both images is not correlated due to the increased contrast of some areas in the postcontrast volume. MR registration could also be performed using temporal images; that is MR volumes taken at different times, typically a period of several months to a year. In this case, misalignment is likely to be larger due to patient reposition, different MR acquisition parameters, and use of breast compression. A pair of slices from temporal MR volumes is shown in Fig. 14.3, along with the difference image where darker areas indicate larger misregistration. Although examples are shown using slices, MR registration

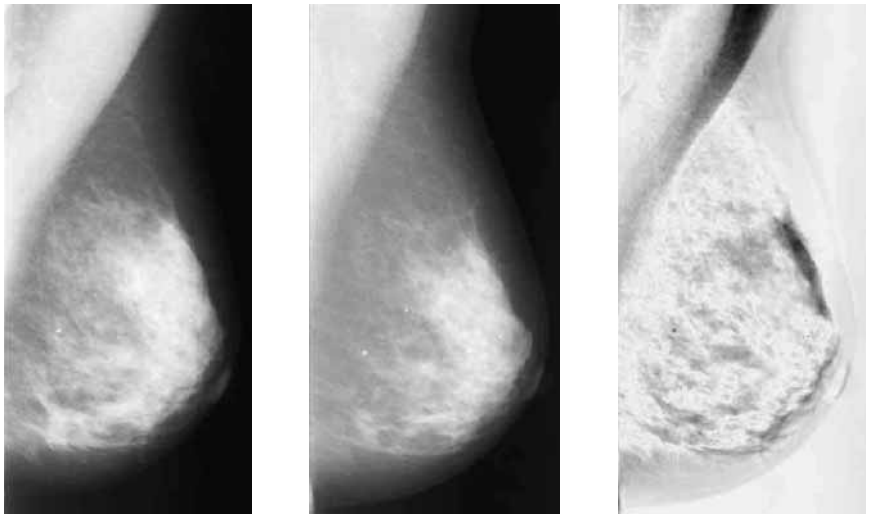

(a) (b) (c)

Figure 14.2 An example of temporal mammograms: (a) reference, (b) target, and (c) difference images.

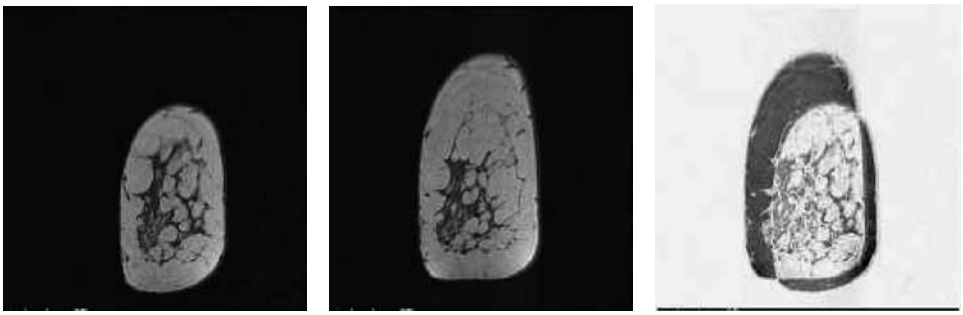

(a) (b) (c)

Figure 14.3 An example of temporal MR volumes: same slice number from the (a) reference, (b) target volumes, and (c) difference image.

is tackled in this chapter as a 3D registration problem. A large misregistration is found that can be described in terms of both global and local distortions.

14.2.1 POINT-BASED METHODS

The use of various registration methods based on correspondence between control-point is covered in this section.

14.2.1.1 2D local affine

A 3D affine transformation is described by 12 parameters

$$\begin{pmatrix} x' \\ y' \\ z' \\ 1 \end{pmatrix} = \begin{pmatrix} a_x & a_y & a_z & t_x \\ b_x & b_y & b_z & t_y \\ c_x & c_y & c_z & t_z \\ 0 & 0 & 0 & 1 \end{pmatrix} \begin{pmatrix} x \\ y \\ z \\ 1 \end{pmatrix}, \tag{14.1}$$

where t_x, t_y, and t_z are translation values and a_i, b_i, and c_i are the transformation parameters responsible for rotation, scaling, and shearing.

In 2D, the number of parameters is reduced to six; therefore, the computation of the transformation parameters needs at least three corresponding control points. Using three control points, a global affine registration is obtained. A local approach can be achieved by having a larger number of control points and solving the affine transformation at each pixel using its three closest control points.

14.2.1.2 2D thin-plate splines

Thin-plate splines (TPS) are a type of radial basis function that was popularized by Bookstein.[7] TPS solves mapping between a set of 2D points by minimizing a measure of bending energy on a thin-plate surface, given by

$$\iint_{R^2} \left[\left(\frac{\partial^2 f}{\partial x^2} \right)^2 + 2 \left(\frac{\partial^2 f}{\partial x \partial y} \right)^2 + \left(\frac{\partial^2 f}{\partial y^2} \right)^2 \right] dx dy, \tag{14.2}$$

where f is the mapping function. This function ensures that $f(x_i, y_i) = p_i$ for all control points p_i and performs interpolation for all the other values. The mapping function is given by

$$\begin{aligned} f_x(x, y) &= a_x x + a_y y + t_x + \sum_{i=1}^{N} w_i U(|\vec{p}_i - (x, y)|) \\ f_y(x, y) &= b_x x + b_y y + t_y + \sum_{i=1}^{N} w_i U(|\vec{p}_i - (x, y)|), \end{aligned} \tag{14.3}$$

where $a_x, a_y, t_x, b_x, b_y, t_y$, and w_i are the deformation parameters, N is the number of points, $\vec{p}_i$ is the ith control point, (x, y) is any point, and U is the thin-plate surface equation defined as

$$U(r) = r^2 \log r^2. \tag{14.4}$$

Thin-plate splines assure piecewise nonlinear registration and have been used in different registration algorithms applied to digital mammography.[1–4,16]

14.2.1.3 Control points

These methods rely on defining sets of control points that provide correspondence between images. The first issue that arises when using point-based methods is the number of control points needed for an accurate registration. Initial results show that a number of control points from 16 to 20 achieves good registration results, while increasing the number of control points does not result in a more accurate registration. This fact is shown in Fig. 14.4, which plots the similarity between original and registered images using mutual information related to the number of control points with local affine and thin-plate spline methods. Local affine transformation achieves poorer measures than the thin-plate splines-based method. The same conclusion is reached using other similarity measures: normalized cross-correlation, entropy of the difference image, and mutual information computed from co-occurrence matrices.[32]

14.2.1.4 3D elastic-body splines

A 3D elastic model was proposed in Ref. 17, called the elastic-body spline (EBS). The model is based on the Navier equilibrium partial differential equation (PDE), which describes a homogeneous isotropic elastic material subject to a force field. EBSs are obtained as a linear combination of translated versions of the solution of the Navier PDE, subject to a smooth force field. Forces at each dimension are described as a 3D thin-plate spline, which ensures the smoothing constraint. Displacements are given by

$$\vec{d}(\vec{x}) = \sum_{i=1}^{N} G(\vec{x} - \vec{p}_i)\vec{c}_i + A\vec{x} + \vec{b}, \tag{14.5}$$

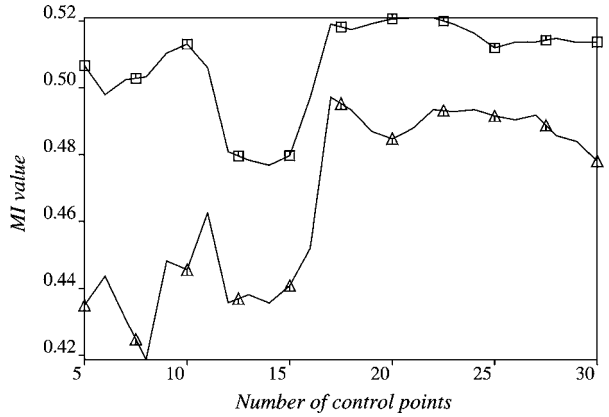

Figure 14.4 Comparison between local affine (△) and thin-plate splines (□) registration related to the number of control points, using mutual information.

where $G(\vec{x} - \vec{p}_i)\vec{c}_i$ is the solution of the Navier PDE for a given 3D point $\vec{p}_i$, subject to a force $\vec{f}(\vec{x}) = \vec{c}|\vec{x}|$, $\vec{c}_i$ are the deformation coefficients, and $A\vec{x} + \vec{b}$ is the affine part that describes the EBS behavior away from the control points (at infinity). This equation is very similar to the function defined for TPS in Eq. (14.3). The main difference lies in the definition of G (a 3×3 matrix), which for EBS is defined as

$$G(\vec{x}) = [\alpha|\vec{x}|^2 I - 3\vec{x}\vec{x}^t]|\vec{x}|, \tag{14.6}$$

where α is the Poisson ratio that is related to the elastic characteristics of the material and I is the 3×3 identity matrix. The applied force field is not unique, $\vec{f}(\vec{x}) = \vec{c}/|\vec{x}|$ has also been proposed resulting in a different solution that is stated to obtain more accurate results. Similarly, other spline transformations can be described using the same approach, just by redefining the function G. This is the case for a 3D version of thin-plate splines ($G(\vec{x}) = |\vec{x}|I$) and for volume splines ($G(\vec{x}) = |\vec{x}|^3 I$).

In Ref. 17, the authors applied the approach to the registration of MR images using manually placed control points. They stated that EBS performed better than 3D thin-plate and volume splines using the same number of control points. Similar experiments to the 2D TPS case showed that the number of control points needed for a satisfactory registration lies between 20 and 30, which agrees with the number of control points used. Registration is performed manually by selecting control points and applying EBS. The selection of control points from a 3D volume is an even more tedious task than for the 2D case.

14.2.2 MUTUAL INFORMATION-BASED METHODS

Registration using maximization of mutual information (MI) has been shown to be very efficient when applied to rigid[18–20] and nonrigid[12,21] registration. The common factor in these approaches is that they find the transformation parameters by optimizing the mutual information measure between images. The cost function for mutual information (MI) is described as

$$F(\alpha) = C[A, T_\alpha(B)], \tag{14.7}$$

where α denotes the transformation parameters and $C(A, B)$ is the MI measure between images A and B. The optimal parameters are obtained by maximizing the above function

$$\alpha = \max_\alpha [F(\alpha)]. \tag{14.8}$$

14.2.2.1 Mutual information

Mutual information,[18,19] based on Shannon's information theory concepts,[22] measures the amount of information a random variable (A) can predict from another random variable (B). In the case of variable independence [$p_{AB}(a, b) = p_A(a)p_B(b)$], MI is minimal as it measures the distance between the joint variable distribution. MI is determined by

$$C(A, B) = \sum_{i=0}^{I} \sum_{j=0}^{J} p_{AB}(i, j) \log \frac{p_{AB}(i, j)}{p_A(i)p_B(j)}, \tag{14.9}$$

where p_A and p_B are the marginal probability distribution of the random variables A and B, respectively; p_{AB} is their joint probability distribution; and I and J are the number of graylevels (or histogram bins) used in images A and B, respectively. Applied to images, each image is identified as one random variable; therefore, it can be determined that the similarity of one image to another by using Eq. (14.9). In this case, probabilities are obtained from normalized marginal and joint histograms.

Since the above measure is dependent on the amount of image overlap, the normalized mutual information is used[12] because it is independent of the number of overlapping pixels in both images and is given by

$$\overline{C(A, B)} = \frac{C(A, B)}{\sum_i^I p_A(i) \log \frac{1}{p_A(i)}}. \tag{14.10}$$

Mutual information has proved to be very efficient in measuring the spatial correspondence between objects[23] and it has been used as a basis of multimodal registration algorithms.[12,15,18,21,24] Mutual information does not rely on intensity relationships between images, instead it is based on statistical properties between two random variables. This issue is of significant importance when working with multimodal images.

An important issue that arises when using mutual information on small or subsampled images is the statistical weakness of the mutual information measure. This is due to interpolation artifacts, which may affect the intensity distribution and, therefore, the mutual information. These problems are more pronounced when using small images and a large number of bins for the joint histogram. Interpolation artifacts can be avoided by oversampling the images, using a higher-order interpolation, or modifying the intensity distribution in order to minimize interpolation effects[21] (i.e., apply random resampling or a prior-joint probability).

Maximization of mutual information can be applied on a global or local basis. A global approach solves the transformation function for the whole image, while a local method recovers different deformations locally. The latter has a higher computation cost, but is able to deal with local distortions.

14.2.3 HYBRID APPROACH

It is possible to combine thin-plate splines and mutual information. Thin-plate splines achieve good registration results, but their main weakness is the tedious and difficult task of establishing point correspondence. Mutual information has been shown to be a reliable similarity measure to use in image registration, but the computational cost involved in finding transformation parameters in complex deformations becomes prohibitive in some applications.

The developed method automatically establishes control-point correspondence using mutual information and then recovers breast deformation using these points in the thin-plate splines algorithm. This process is based on a multilevel approach for which a two-level example is illustrated in Fig. 14.5. At the first level, the whole corresponding images (named reference and warped) are rigidly aligned, obtaining the transformation parameters α_1. Subsequently, at the second level, each mammogram is divided into six rectangular subimages, and each subimage is rigidly aligned to its corresponding subimage. Note that transformation parameters are carried through each level, assuming that each subimage at a lower level would suffer a different transformation, but are related to the deformation at the higher level. Assume this speeds up the optimization process as well as avoiding local minima situated away from the optimum solution. Once the last level is reached, point correspondence is extracted from corresponding subimages (i.e., the center pixel), assuming that in such small subimages the local nonrigid deformation is very small and can be ignored.

To ensure a correct correspondence, the following constraints are imposed on the control points:

(1) The distance between each point in the warped image, before and after transformation, has to be smaller than a threshold D, which is set to the maximum size of the subimage.
(2) Subimage correspondence would be taken into account if the similarity between subimages is higher than a given threshold S.

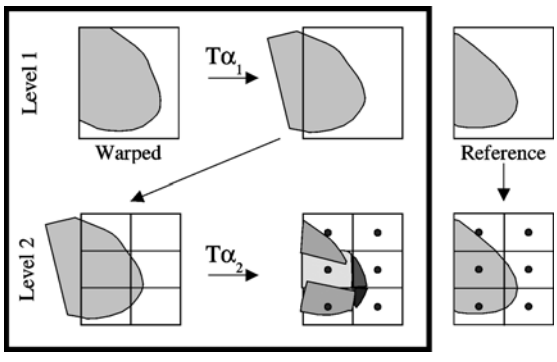

Figure 14.5 Point correspondence using multilevel mutual information.

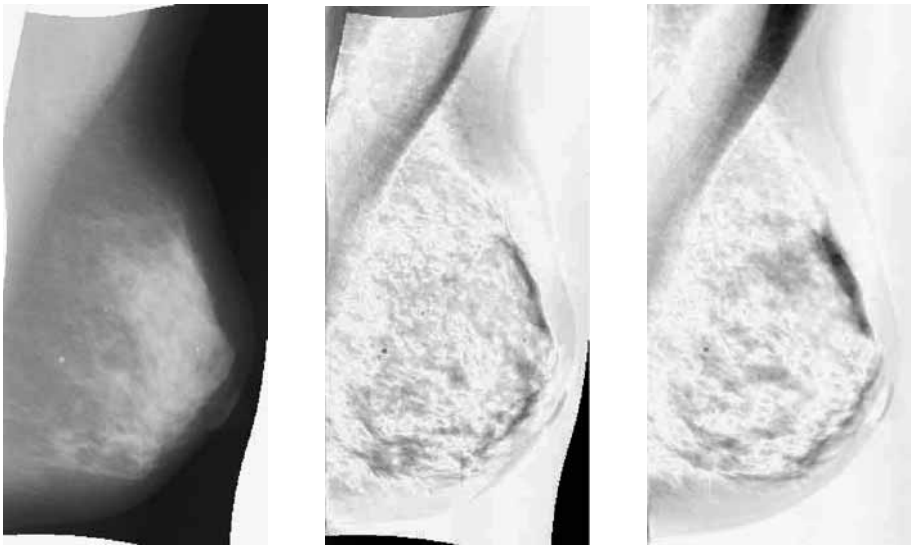

(a) (b) (c)

Figure 14.6 Temporal registration using multilevel mutual information and thin-plate splines: (a) registered; (b) difference; and (c) original difference images.

A similar algorithm was also proposed[21] for the nonrigid correspondence in muscle fiber images. The approach used here is similar, with the main difference being that the thin-plate algorithm is applied at the end of the multilevel process, and not at each level. It is our assertion that the use of thin-plate splines at each level can have a negative impact on the registration accuracy by increasing interpolation errors. Once correspondence points have been found, they are used to recover the deformation using thin-plate splines. Figure 14.6 shows an example of this method applied to mammographic registration. Registration results using this approach are found to be less accurate than using thin-plate splines with manually placed control points, although it is certainly better than the unregistered case and using a global affine transformation. This illustrates how landmark placement affects registration accuracy in point-based methods. The lower accuracy is because automatic landmarking with mutual information establishes good point correspondence, but it does not use the most representative points, such as internal structures or salient regions, as is done in manual landmarking. Therefore, the next step to the automatic landmarking proposed here would be to identify more salient points (not using subimage centers as were used so far), which would be obtained using feature detection methods (see Section 14.3).

14.2.4 EVALUATION

Initial registration results based on 19 sets of temporal x-ray mammograms using three of the methods previously described (local affine, thin-plate splines, and

global affine using mutual information) are discussed here. Figure 14.7 shows similarity measures between registered and reference images using four similarity metrics: normalized cross-correlation, entropy of the difference image, mutual information, and mutual information computed from co-occurrence matrices.[32] For all (except entropy), a higher (lower) measure indicates higher similarity. As expected, thin-plate splines obtain a better overall result. The local affine transformation achieves good registration results, but its overall performance is lower since it contains some discontinuous deformations and does not account for nonlinear deformations.

A summary of those results is shown in Table 14.1, which computes various statistics obtained from Fig. 14.7. In all cases, the conclusion is that thin-plate splines is the method that obtains the most accurate results (i.e., high similarity measures). In addition, it can be concluded that the cross-correlation measure does not produce results independent of the registration method, which is more so with the other measures. Finally, the MI measure provides the most stable results overall.

The evaluation experiment above is based on the assumption that a better similarity measure (e.g., a higher value for mutual information) accounts for a better registration (i.e., the registered images are more similar). One could argue that this will not be always the case, and a higher measure of similarity could mean a registration of worse quality. Although difficult to validate, the following experiment was conducted to determine if there is a correlation between objective measures of similarity (e.g., mutual information) and assessment by a human observer. The images used are the same as those used in the previous experiment shown in Fig. 14.7. The observers were presented with three registered images obtained with the three methods under evaluation (global and local affine transformation and thin-plate splines) for each of the 19 cases. The registration results were presented in random order next to each other. They were asked to rate the three images, from what they considered to be the best quality registration to the worst. For each registered im-

Table 14.1 Evaluation of image registration approaches: mean and standard deviation of various similarity measures evaluating global affine using MI (Global AT), local affine (Local AT), and thin-plate splines (TPS). Similarity measures used are normalized cross-correlation (CC), entropy of the difference image (EN), mutual information (MI), and co-occurrence-based mutual information (CM).

CC	**Mean**	**StDev**	**EN**	**Mean**	**StDev**
Global AT	0.932	0.047	Global AT	1.551	0.129
Local AT	0.767	0.229	Local AT	1.606	0.157
TPS	**0.955**	**0.028**	**TPS**	**1.474**	**0.119**
MI	**Mean**	**StDev**	**CM**	**Mean**	**StDev**
Global AT	0.427	0.086	Global AT	0.442	0.062
Local AT	0.434	0.081	Local AT	0.463	0.056
TPS	**0.514**	**0.0531**	**TPS**	**0.504**	**0.049**

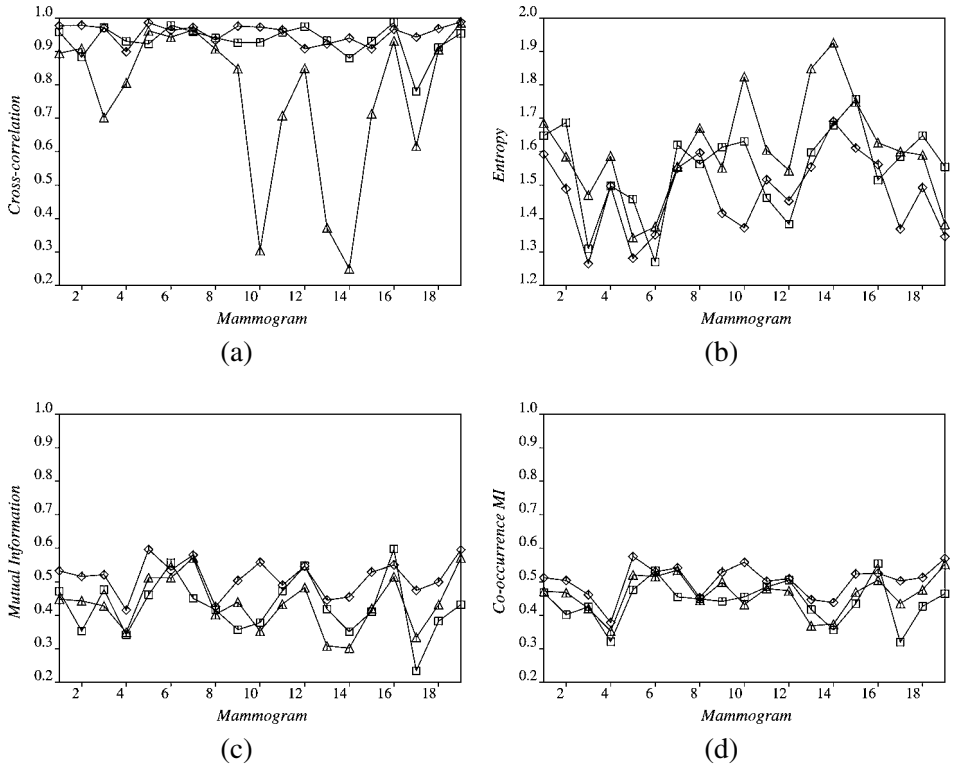

Figure 14.7 Evaluation of image registration approaches: global affine using MI (□), local affine (△), and thin-plate splines (◇), using (a) normalized cross-correlation, (b) entropy of the difference image, (c) mutual information, and (d) co-occurrence-based mutual information.

age, the observer could choose to see the registered image (aiming to match the reference image), and the difference image between the registered and the reference images. They could assess the transformation function using the registered image (i.e., smoothness, continuity, large distortions, etc.) and spot misregistered areas using the difference image. Figure 14.8 shows the result of the observer experiments. Three different observers familiar with mammographic images but not experienced radiologists, took part in the experiment. Each observer did the observation twice to minimize their variability.

Results show a similar trend compared to the similarity measures obtained in Fig. 14.7. For instance, the better quality of registration in mammogram six for the global affine transformation is captured by all similarity measures. In addition, and although a perfect agreement with the human observer is not always achieved, graphs show similar trends, e.g., in case 12 where global and local affine have similar quality (graphs get closer together in Fig. 14.8), which is captured by similar MI measures in Figs. 14.7(c) and (d).

Table 14.2 summarizes the results obtained in the observer study. This shows a confusion table for each similarity measure where the human classification or-

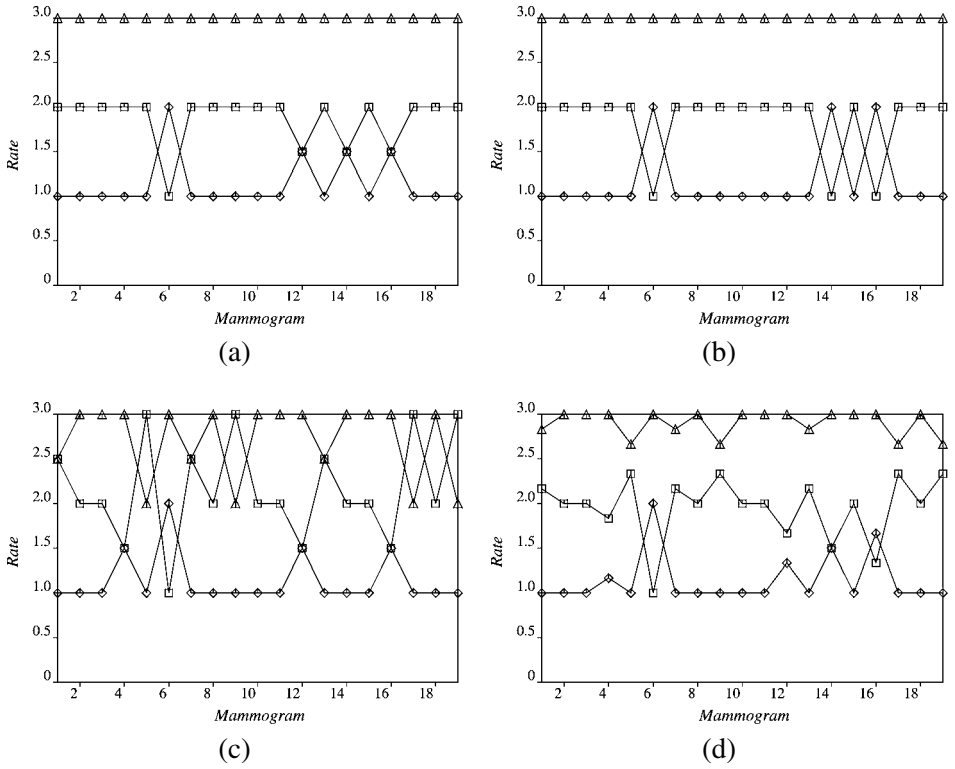

Figure 14.8 Observer study, evaluation of image registration approaches: global affine using MI (□), local affine (△), and thin-plate splines (◇), by three different observers (a), (b), (c), and their mean in (d).

der is compared to those based on the various similarity measures. The presented results show higher correct classification rates for the cross-correlation and mutual-information-based measures. However, without taking the local affine transformation case into account (which human observers agreed had the worst results), mutual-information-based measures obtain the highest correct classification rates (76% and 74% for MI and CM measures, respectively) compared to CC and EN measures (66% and 61%, respectively). These results agree with the conclusions drawn above. In addition, the fact that mutual information does not rely on the intensity correlation between images is regarded as an advantage compared to measures such as cross-correlation, when used in multimodal applications.

14.2.5 SUMMARY

Various registration approaches have been evaluated and their suitability to be used in mammographic registration has been investigated. The obtained results agree with our initial belief that a nonparametric model (thin-plate or elastic-body

Table 14.2 Observer study: confusion tables for each similarity measure with human observer as ground truth, where GAT is global affine transformation, LAT is local affine transformation, TPS is thin-plate splines, CC is 41/57 (72% correct), EN is 35/57 (61% correct), MI is 39/57 (68% correct), and CM is 37/57 (65% correct).

		1	2	3		1	2	3		1	2	3
CC	1	0	0	0	1	12	0	0	1	2	5	0
	2	0	0	3	2	5	2	0	2	0	9	0
	3	0	0	16	3	0	0	0	3	0	3	0
		1	2	3		1	2	3		1	2	3
EN	1	0	0	0	1	12	0	0	1	3	6	0
	2	0	0	7	2	4	3	0	2	0	5	0
	3	0	0	12	3	0	0	0	3	0	5	0
		1	2	3		1	2	3		1	2	3
MI	1	0	0	0	1	17	0	0	1	2	0	0
	2	0	0	9	2	0	2	0	2	0	8	0
	3	0	0	10	3	0	0	0	3	0	9	0
		1	2	3		1	2	3		1	2	3
CM	1	0	0	0	1	17	0	0	1	2	0	0
	2	0	0	10	2	0	2	0	2	0	7	0
	3	0	0	9	3	0	0	0	3	0	10	0
		LAT				**TPS**				**GAT**		

splines) is needed to deal with the complexity of the breast deformation in both x-ray and MR images. This has been assessed using x-ray images, but can also be extrapolated to MR and, moreover, agrees with conclusions drawn by other authors.[2,12,13,17] The nonparametric models investigated obtained accurate results, but care has to be taken in selecting control points. An automatic correspondence method has been described based on a multilevel mutual-information method that yields promising results. The main bottleneck of the described approach, which is the automatic selection of salient control points, is further discussed in the next section.

14.3 IDENTIFYING SALIENT LINEAR STRUCTURES

Extraction of features, that describe an image or parts of it, plays a crucial role in the success of image registration, or any other process that makes use of those features. This section reviews various approaches used for feature extraction in medical applications, placing special emphasis on mammographic features. A novel approach to the extraction of robust features from x-ray (2D) mammographic images is presented. Feature extraction applied to MR (3D) images is also described following a similar methodology to the 2D case.

14.3.1 MAMMOGRAPHIC FEATURES

Various approaches have been developed to extract characteristic features from mammographic images. Those features include the breast boundary, nipple, pectoral muscle, parenchymal tissue, and internal (blob and linear) structures.

The breast outline is one of the most commonly used features in the registration of mammographic images since it provides valuable information about the breast in terms of deformation and volume. In addition, other features are extracted from the boundary, such as the nipple, rib cage, or axila positions. Simple global thresholding has often been used to separate the breast from the background. However, other approaches have been proposed; for example, in Ref. 25 the authors model the gray-level distribution of the mammographic background using a second-order polynomial and then subtract it from the original image.

In this work, the breast boundary is extracted using a similar approach as in Ref. 26. Global thresholding and morphological opening (using an octagonal structuring element) are applied to the images. The breast boundary is obtained by extracting the largest region in the image.

A common approach to detecting the nipple position is to regard its position as a point of high local curvature in the breast outline.[4,27] However, in some mammograms, the nipple does not show up in the breast profile and therefore cannot be accurately extracted. Based on the curvature of the breast outline, other features are also obtained such as the rib cage and axila points,[4] but as before, those points may not be visible in all cases. Extraction of the pectoral muscle has been used in order to isolate the breast region from the bright pectoral area. This is useful to limit the processing area of certain methods (e.g., breast boundary points for image registration as in Ref. 26). However, abnormalities may develop in the pectoral muscle area; therefore, for abnormality detection systems, a removal of such areas is not always a satisfactory solution. The pectoral muscle area usually corresponds to the brighter, approximately triangular area in the top left of the mammogram (top right for a right mammogram). Generally, two approaches have been used: detection of a straight line at a given orientation and image thresholding. As an example of the former, a Hough-transform-based method has been successfully used to remove the pectoral muscle in a parenchymal-tissue-classification method.[28] In Ref. 26, the pectoral muscle is extracted by image thresholding and posterior opening using a triangular structuring element. However, other approaches[3] incorporate the pectoral area as part of the breast region and perform intensity transformation (i.e., using a distance transform) in order to remove the characteristic brightness of this region.

Extraction of internal features from the breast region has also been an important research subject. In Ref. 29, a review and comparison of various ridge (or line) detection methods applied to mammography is given, concluding that best results are obtained using orientated bins and the nonlinear line operator.

A multiscale wavelet analysis has been used by Ref. 4 for the detection of internal breast regions and used for mammographic registration.

In Ref. 5, the authors extract internal regions that maximize a saliency metric related to isointensity areas. Correspondence between regions in different mammograms is obtained. Hence, salient regions where a correspondence has not been found are likely to be related to recently developed areas that could be due to an abnormality.

Salient points are obtained in Ref. 6 where the authors extract points of correspondence between mammograms based on finding a matching of features extracted from the crossing of horizontal and vertical linear structures.

In the next section, a feature-extraction method for mammographic images is described. The proposed method uses both linear structures from the breast boundary and from the breast region (i.e., ducts, vessels, fibrous tissue, and pectoral muscle). A distinction between boundary and internal structures is made because boundary information is used to restrict the detection area of internal structures. This results in faster (applying detection to a smaller area) and more robust (avoiding mammographic artifacts) detection.

14.3.2 INTERNAL LINEAR STRUCTURES

The detection of internal linear structures is approached using a nonlinear line operator.[29] At a given scale, the line operator provides a strength and orientation of the linear structure for every pixel. Line strength is obtained by comparing the mean gray level from a straight line of pixels with its neighborhood, and obtaining the maximum value from a number of orientations. Direction of the line strength is determined by the angle of the line that gives the highest line strength. In addition, scale information can be obtained from the maximum line strength of the detector at different scales. An example of the application of the line operator to mammographic images is shown in Fig. 14.9(b).

14.3.2.1 Line processing

Once line strength, direction, and scale information have been obtained, different operations are performed to facilitate the feature-extraction process. First, a conservative threshold on the line-strength image is set in order to remove background

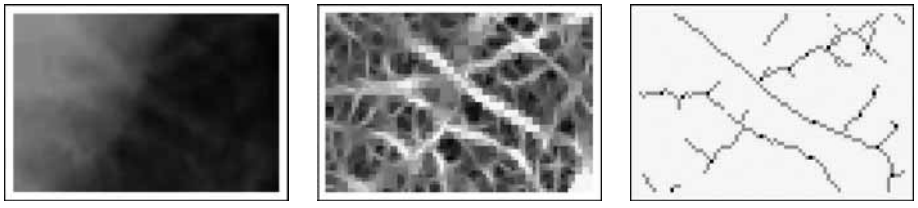

(a) (b) (c)

Figure 14.9 Feature extraction: (a) original mammogram, (b) detection of linear structures, and (c) extracted linear structures (gray) and curvature points (black).

noise. Nonmaximum suppression is then applied, which removes pixels with low intensity values compared to their neighbors along the normal of the linear structure. Scale information extracted from the line operator is used here to determine the position of candidate pixels to be suppressed. In addition, short lines that do not provide valuable information are removed. Finally, a thinning operation (based on preserving pixel connectivity) obtains the backbone of the most representative linear structures in the mammograms. Figure 14.9(c) shows thinned linear structures obtained from a region of a mammogram using the above processing.

14.3.3 FEATURE EXTRACTION

After obtaining the salient linear structures, extraction of features is needed in order to have descriptors of such structures. Features used in the literature include line strength (contrast),[30] line width,[30,31] line length,[31] orientation,[30,31] curvature,[33] corners,[34] crossing points,[33] and end points.[30,31,33] Corresponding linear structures in two mammograms can present large differences related to line strength and line continuity (due to different radiation exposure and breast compression), but width and orientation of the line and local curvature and branching points are more likely to be preserved, and often are features used by radiologists when comparing mammograms. Therefore, features that take line length, end points, and line strength into account turn out to be unreliable features to be used in a correspondence approach. Here, local features such as curvature, width, and orientation are used. The basic idea of the developed approach is to extract characteristic points of linear structures determined by their maximal local curvature along the linear structure. Examples of such points are shown in Fig. 14.9(c). It should be noted that branching points and corner points are detected, but not end points.

Curvature values at each pixel are obtained with a similar approach as used in Ref. 33. Curvature (or directional change) between two pixels p and q is defined by the scalar product of their normal vectors. Hence, the curvature measure of a given pixel p is obtained by computing the scalar product between p and its neighboring pixels,

$$C_p = \frac{1}{N}\sum_{i=1}^{N} \exp\left(-d_{ip}^2\right)\left[1 - \cos(\phi_p - \phi_i)\right], \tag{14.11}$$

where ϕ_i is the angle of the normal at a pixel i. Since curvature is going to be extracted from binary thinned images, unit vectors are assumed. N is the number of points in a local neighborhood and d_{ip} is the Euclidean distance between points i and p. The distance factor is used here to weight the curvature of each point i, in order to incorporate a bias to points closer to p.

Position, orientation, and width are then extracted from those points that are to be used in the matching process described in Section 14.4. Orientation is obtained directly from the thinned linear structures, while width is extracted after nonmaximum suppression of the line strength images as described in Section 14.3.2.

The width of a linear structure at a point is given by the number of pixels along the normal of the structure until a nonstructure pixel is found.

14.3.3.1 Initial results

Corresponding linear structures are likely to suffer local distortions between images taken at different times, but it is believed that the local features such as the ones described will remain similar. Figure 14.10 shows thinned linear structures extracted from areas of the same mammographic images, where one of the images has been deformed using a nonlinear transformation using TPS (based on real results from a temporal registration). In addition, maximum curvature points are also shown depicted by a darker color. Although corresponding lines present different distortions and broken structures, an overall similarity should be clear.

Using the same example, a different area is shown in Fig. 14.11 that includes width and orientation information extracted from the linear structures. Black lines represent normal vectors of the linear structure at a maximum curvature point. The length of the normal is related to the width of the linear structure. It can be seen from both Figs. 14.10 and 14.11 that curvature points and features extracted at those points remain fairly constant. This illustrates that the points extracted using

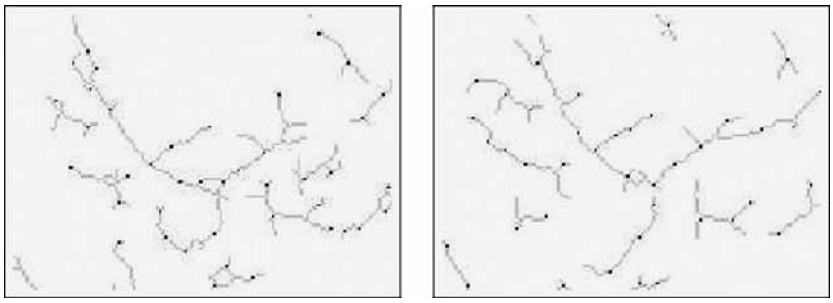

Figure 14.10 Extracted linear structures (in gray) and points of maximum curvature (in black) from two mammographic images: original (left) and deformed (right).

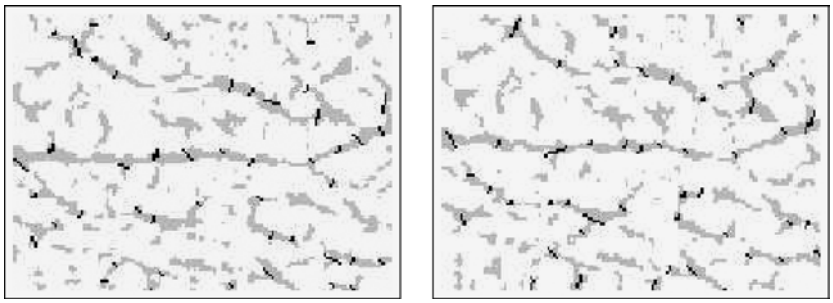

Figure 14.11 Width and orientation features obtained from linear structures from two mammographic images: original (left) and deformed (right).

the described approach can be invariant to realistic nonlinear transformations, and therefore used in a correspondence approach.

14.3.4 EXTENSION TO 3D

So far, the feature-extraction process has been applied to 2D x-ray images. Here the use of the same principle applied to 3D images, such as MR images are investigated. This involves the extension of a number of the techniques to 3D, such as the line operator and line processing, which are described below.

14.3.4.1 3D line operator

The idea behind the line operator in 2D has been extended to the detection of lines in 3D images. At a given orientation, the line strength at a voxel is defined by the difference between neighboring voxels (in a 3D neighborhood) and voxels along the line. The final pixel strength is obtained by extracting the maximum value for all orientations. The orientation where the maximum is obtained is also describe the orientation of the line at that voxel. Line orientation is defined as the tangent angle of the line, and it is represented in spherical coordinates by two angles (ϕ and θ), which are related to a 3D rotation along the y- and x-axes, respectively. As in the 2D case, the operator can be applied at different scales. This is achieved by recursively subsampling the image (using Gaussian convolution) and applying the kernel at each scale.

14.3.4.2 Line processing

Similar to the 2D case, after setting a conservative threshold, nonmaximum suppression is applied. In the 3D case, voxels are removed if they have a lower intensity value compared to their neighbors following the orthonormal directions ($\vec{u}$, $\vec{v}$) to the tangent vector $\vec{t}$ along the linear structure as depicted in Fig. 14.12. Subsequently, a 3D-thinning operation is performed in order to obtain the backbone of the linear structure. The algorithm has been developed based on existing 2D thinning approaches.

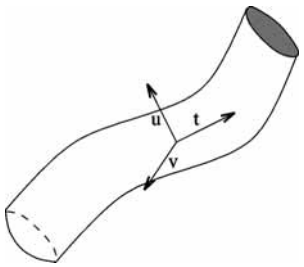

Figure 14.12 Directions involved in the 3D nonmaxima suppression: $\vec{u}$ and $\vec{v}$ are the orthonormal vectors to $\vec{t}$, the tangent vector to a voxel in the linear structure.

14.3.4.3 Feature extraction

The extraction of salient points from the 3D-thinned volume is based on the same local line curvature definition presented for the 2D case [see Eq. (14.11)]. Local curvature is defined by computing the tangent disparity using the vector dot product of tangent vectors (again assuming unit vectors):

$$C_p = \frac{1}{N}\sum_{i=1}^{N} \exp\left(-d_{ip}^2\right)\left(1 - \vec{t_p} \cdot \vec{t_i}\right), \tag{14.12}$$

where $\vec{t_p}$ is the tangent vector of voxel p.

Finally, two width measures are obtained for each voxel, given by the number of nonzero pixels in the $\vec{u}$ and $\vec{v}$ directions (see Fig. 14.12) from the nonmaximum suppression image.

14.3.4.4 Initial results

Results of the 3D extraction process are shown in this section. For display purposes, some of the examples are shown as slices, but it should be emphasized that the whole process is performed in 3D. An example of feature extraction applied to MR images is shown in Fig. 14.13. Figures 14.13(a)–(c) show a line strength image obtained using the line operator. The small size of the MR images (at most a region of approximately $150 \times 150 \times 50$ voxels) limited the use of a large range of scales for the line detector. Therefore, in the remainder of this chapter, two different scales have been used.

Figure 14.13(b) shows a slice obtained after nonmaximum suppression, showing the extend of the linear structures. A volume rendering of the thinned linear structures is shown in Fig. 14.13(c). Finally, in Fig. 14.13(d) maximum local curvature points are obtained. Although difficult to assess, the obtained points can be seen to describe internal linear structures with a homogeneous distribution.

14.3.5 SUMMARY

This section has reviewed different approaches for the extraction of features in images. It has focused on the detection of edges and ridges, with special emphasis on medical applications. A methodology for the extraction of salient points in x-ray images has been presented based on extracting points of maximal local curvature along the linear structures. Evaluation has shown that those are stable points. In addition, the methodology has been extended to MR (3D) images based on the same principles. In this case, a 3D-line detector has been developed based on a previous approach used for 2D images. Although of higher computational cost compared to other edge/ridge detectors, initial results are promising. It is believed that it could provide higher response in noisy images since has been reported to

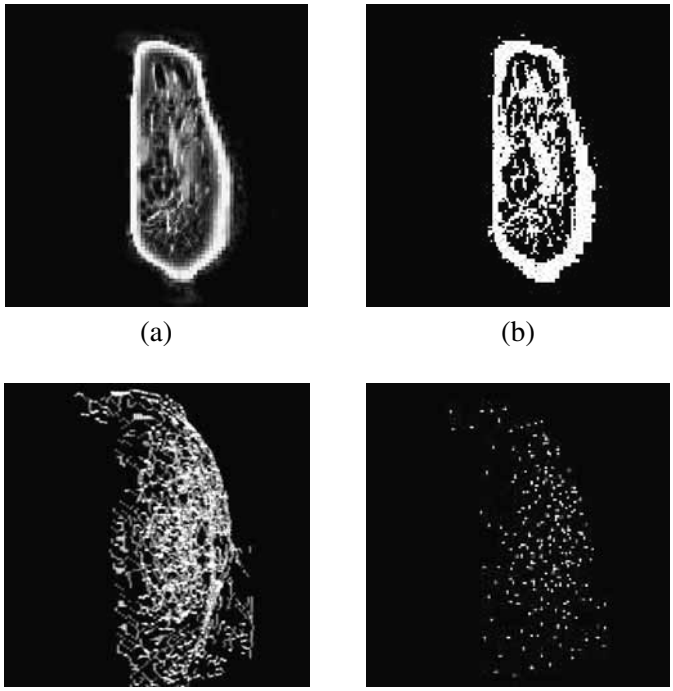

Figure 14.13 Feature extraction applied to a 3D MR volume: (a) line strength from the line operator. Salient points are shown in (d) after performing nonmaximum suppression (b) and thinning (c).

do so with the 2D case. In the extension to the third dimension, the postprocessing step has been described stating the major differences compared to the 2D case.

14.4 REGISTRATION USING LINEAR STRUCTURES

The problem of establishing line correspondence in mammograms involves various steps: (1) identifying linear structures in both mammograms, (2) extracting reliable information from those structures, and (3) obtaining correspondence between the structures based on the best match of the information previously extracted (see Section 14.4.1). Detection of linear structures and feature extraction were described in the previous section. Those features from the linear structures are used by a matching process to find correspondence between points. Once correspondence has been established, registration can be performed in both mammograms using a point-based method like thin-plate splines.[7] For the tracking application, instead of applying a registration method, a process of identification and matching of linear structures in various images is performed based on the point correspondence. It should be noted that the matching process remains exactly the same for both applications (registration and tracking).

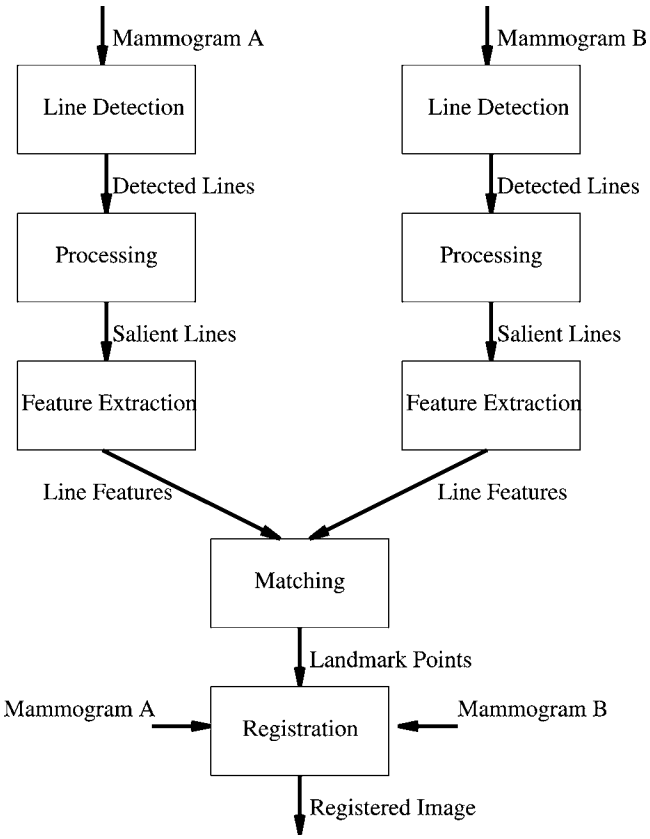

Figure 14.14 Overview of the proposed method.

The matching algorithm is developed using a multiscale approach in order to obtain more robust correspondence (see Section 14.4.1). Figure 14.14 shows an overview of the proposed method.

14.4.1 MATCHING

The feature extraction described in Section 14.3 provided various features obtained from characteristic points on the linear structures. The goal is to establish correspondence between those points in two (or more) mammograms. Matching two sets of feature points is a common problem in computer vision. To minimize computation time, different approaches have been used such as chamfer matching,[35] iterative closest point,[36] and relaxation-based approaches.[30,31] However, all the methods make assumptions that are not applicable to our matching problem (i.e., rigid movement and a geometric relationship between structures). The matching process of two sets of feature points needs to consider the following four assumptions:

(1) *Nonrigid motion*: linear structures in mammograms suffer local distortions; therefore, they may move independently, and no geometrical relationship is established between neighboring structures.
(2) *Multiple matches*: a linear structure in one mammogram can match more than one structure in the other mammogram, and vice versa.
(3) *Nonbijectivity*: a linear structure in one mammogram may not have a corresponding linear structure in the other, and vice versa.
(4) *Localization:* after global breast misalignment is removed, matched linear structures lie in approximately the same area in both mammograms; the localization area M.

14.4.1.1 Method

Here, a similar but more general approach than the one used in Ref. 6 is adopted. The set of feature points from both mammograms are denoted as $\{a_i | 1 \leq i \leq N_i\}$ and $\{b_j | 1 \leq j \leq N_j\}$, where N_i and N_j are the number of feature points used, which may not be the same. Subsequently, a distance matrix (DM) is built in which each position $DM(i, j)$ describes the normalized distance between features of points a_i and b_j. Hence, a low value means good matching between points. The use of the distance matrix structure fulfills the first three assumptions: independent motion (matched points a_i, b_j do not imply matching a_{i+1}, b_{j+1}); a point a_i may have multiple matched points b_j; and a point in either mammogram may remain unmatched.

Satisfying the last assumption, localization, position $DM(i, j)$ only has a finite value if points a_i and b_j are in the same localization area in both mammograms. This assumption can only be stated if both mammograms are globally aligned; that is, global deformation (i.e., rotation, translation, scale, and shear) is removed. Therefore, mammograms are initially registered maximizing a mutual information measure using an affine transformation. The normalized distance is determined by three components. The first distance is the Euclidean distance (D_E) between point coordinates. Coordinates of one of the points are transformed (T_α) using the parameters obtained from the registration mentioned earlier. The second distance is the orientation difference between two points (D_ϕ), similar to the curvature definition in Eq. (14.11). The third distance is the width difference between two points (D_w) normalized using the maximum width of all the linear structures (W). Using equal weighting, the normalized distance is given by

$$\begin{aligned} DM(i, j) &= D_E + D_\phi + D_w \\ &= \frac{|T_\alpha(a_i) - b_j|}{M} + \frac{1 - \cos(\phi_i - \phi_j)}{2} + \frac{|w_i - w_j|}{W}. \end{aligned} \quad (14.13)$$

14.4.1.2 Multilevel approach

A multilevel approach similar to the local affine method described in the previous section (see Section 14.2.3 and Fig. 14.5) is used here to ensure a spread of control points over the whole image and to improve the accuracy of the global registration process. At the first level, the full images are aligned, obtaining the transformation parameters α_1. Subsequently, at the second level, each mammogram is divided into six rectangular subimages and again each subimage is aligned to its corresponding subimage. Note that transformation parameters are carried through each level, assuming that each subimage at lower levels would suffer a different transformation, but it would be related to the deformation on the higher level. Assuming this, the optimization process is sped up and local minima situated away from the optimum solution is avoided. Once the last level i is reached, transformation parameters α_i at each level establish correspondence between structures within the subimages. Extracting the local best matches in each subimage assures that a minimum number of matches are present in each subimage, providing a homogeneous point distribution over the mammograms. This multilevel algorithm is based on the principles of the algorithm described in Section 14.2, but in this case points are obtained from the linear structures instead of using the central pixel of the subimages.

14.4.2 EVALUATION

In this section, different aspects of the matching method applied to mammographic registration are evaluated. In the presented experiments, only normal mammograms, from 10 women were used.

In order to assess the accuracy of the developed approach, a comparison between registration using matches from the author's method and matches obtained manually is given. Subsequently, a framework to detect structural abnormalities in mammograms using information from the registration is proposed.

Figure 14.15 shows two mammograms of the same woman taken three years apart, where matches between the linear structures are indicated by numbers (in white). In addition, manually placed control points (in black) are also shown. It should be noted that points matched with the developed approach follow a homogeneous and coherent distribution that is comparable to the manually placed points.

Figure 14.16 shows the deformation applied (using the developed approach) and subtracted images (where darker areas mean larger misalignment) obtained after registration, using the proposed method [Fig. 14.16(b)] and manual points [Fig. 14.16(c)]. Although misregistration can be observed near the breast outline, registration of the internal breast region is comparable to manual placement of the control points.

Figure 14.17 shows registration results of temporal (same breast taken at different times) and contralateral (right-left comparison) mammograms. Graphs are normalized to manual registration. They show that automatic registration performs equally or slightly better than manual registration in most cases, although some

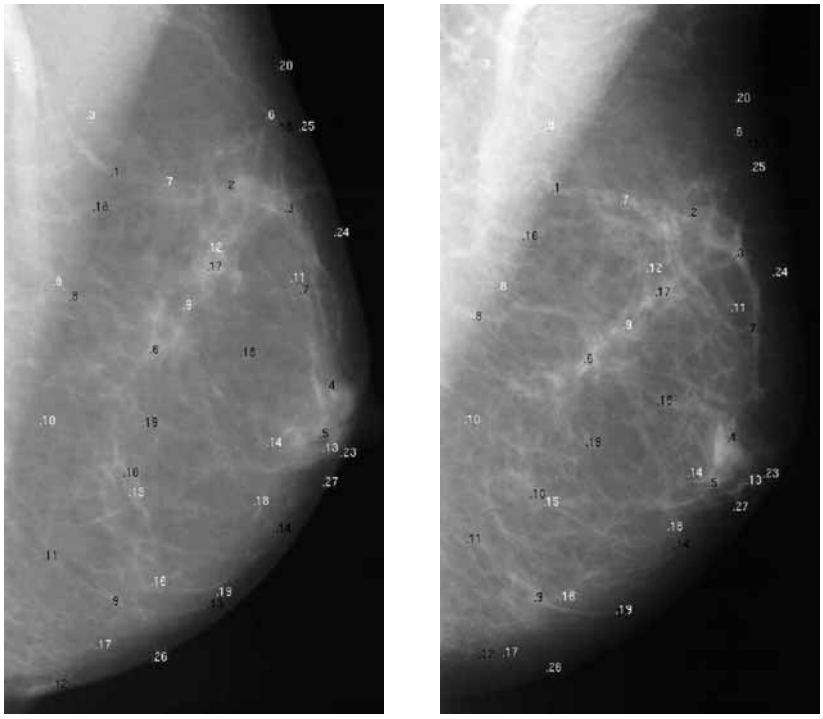

(a) (b)

Figure 14.15 Correspondence between linear structures in temporal mammograms: (a) reference and (b) warped images.

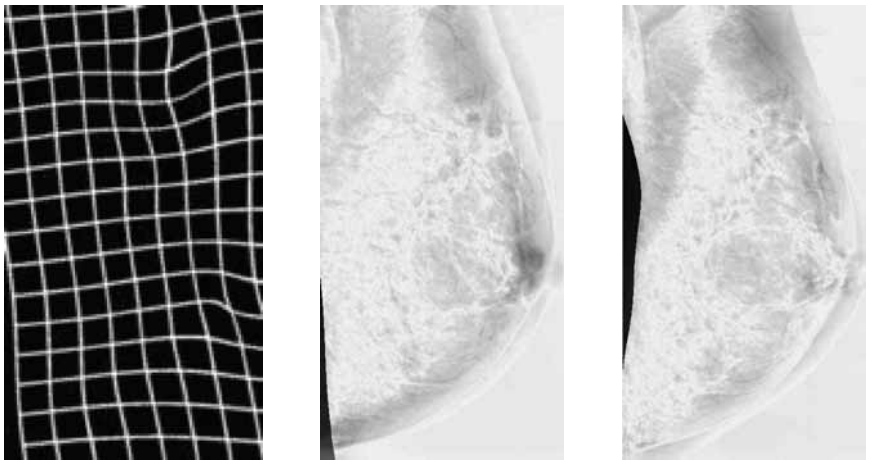

(a) (b) (c)

Figure 14.16 Correspondence between linear structures in temporal mammograms: (a) applied deformation using the proposed approach, difference between registered image and reference based on (b) automatic and (c) manual correspondence.

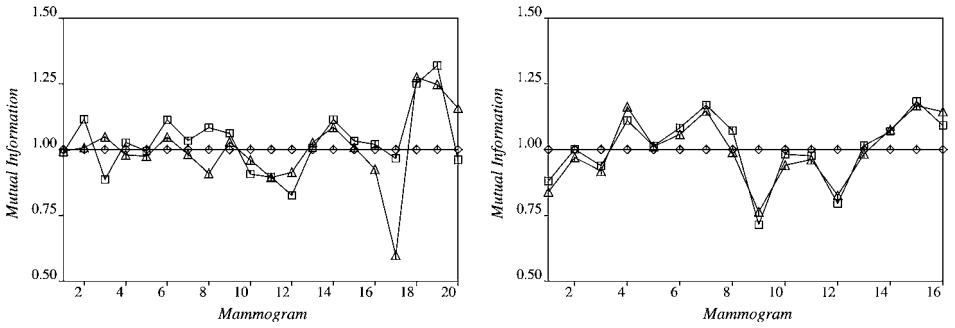

Figure 14.17 Results for (a) temporal and (b) contralateral registration where the proposed method (□) is compared to registration using the breast outline (△) and manual registration (◇).

Table 14.3 Registration results from temporal and contralateral mammograms.

Temporal	Mean	StDev	Contralateral	Mean	StDev
Manual	0.498	0.040	Manual	0.502	0.059
This approach	0.522	0.041	This approach	0.501	0.050
Breast boundary	0.497	0.059	Breast boundary	0.496	0.044

poor results are also obtained. The method is also compared to registration using only the breast boundary, which has been used by other authors. Although similar results are obtained, including internal information achieves a more robust registration.

Table 14.3 shows mean and standard deviation measures of similarity (mutual information) obtained from the temporal and contralateral registration. For the temporal case, the developed approach obtains the highest mean value, whereas in the contralateral case its value is close to the manual registration.

14.5 DETECTION OF ABNORMALITIES

Registration results using the developed approach (in both temporal and contralateral cases) are comparable to manual registration. It is believed that the use of features extracted from the difference image could be used to discriminate between normal and abnormal mammograms. For a normal mammogram, the difference between registered images should be minimal, whereas for an abnormal case it is likely to highlight the abnormal region. An example of an abnormal case is shown in Fig. 14.18, where the right mammogram contains a spiculated lesion. Contralateral registration is performed using the proposed approach. From the difference image after registration [Fig. 14.18(c)], it can be seen that the spiculated lesion is clearly highlighted and misalignment is minimized compared to the original image difference [Fig. 14.18(b)].

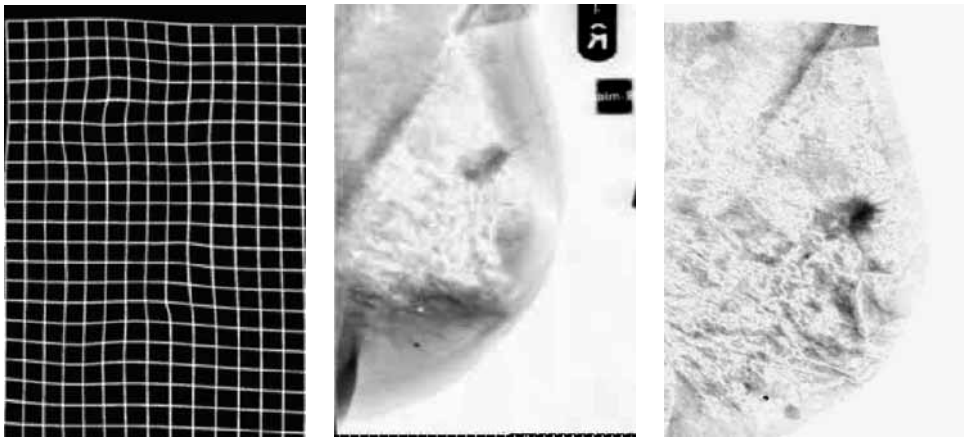

(a) (b) (c)

Figure 14.18 Correspondence in contralateral mammograms: (a) applied deformation and difference images (b) before and (c) after registration.

Registration has been performed on a data set containing pairs of temporal mammograms taken at different screening rounds (with approximately 3 years between each pair—1993, 1996, and 1999). The data set contains 22 women with 12 of them presenting abnormalities (structural distortions or spiculated lesions) in the last screening round.

All the above expectations are confirmed in the results shown in Fig. 14.19, which plots features extracted from the thresholded-difference image in both normal and abnormal cases after registration. For the normal case, similar results are obtained from the three different screening rounds, although decreasing mean values are obtained through the years that could be due to changes in breast density (increase of the fatty tissue). On the other hand, abnormal mammograms in the last screening year (when the abnormality was diagnosed) show high dissimilarities compared to previous years and to normal mammograms. It should be noted that in the early screenings (1993 and 1996), a similar trend to the normal case is obtained for the abnormal mammograms, although slightly higher values are obtained. Features used in Fig. 14.19 are the normalized area and perimeter of the largest region in the difference image. Other features have been tested, obtaining similar but less pronounced results.

In addition, the registration approach can be used to track regions of interest over time; in this case a region containing an abnormal structure. Figure 14.20 shows registered regions of three mammograms taken at different screening rounds (with approximately three years time between each one, i.e., 1992, 1995, and 2000), where an abnormality was diagnosed in the last screening round. Tracking regions is performed by registering the 1995 and 2000 images to the 1992 image, regarded here as the reference image. This shows that the abnormality is only present in the final year, with no mammographic evidence in earlier screening

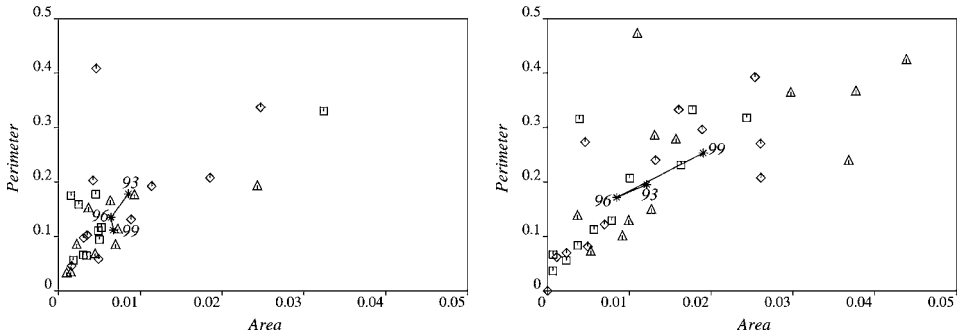

Figure 14.19 Features from registration of normal (a) and abnormal (b) mammograms in several screening rounds: 1999 (△); 1996 (□); and 1993 (◇), and the mean value for each year (∗).

Figure 14.20 Tracking of an abnormal region in mammograms from various screening years: (a) 1992, (b) 1995, and (c) 2000.

rounds. These tracking results could be used as a training tool for radiologists and also to investigate early signs of cancer in the regions prior to the detection of the abnormality.

14.6 TRACKING OF LINEAR STRUCTURES

Tracking objects in image sequences is a well-developed area.[37] However, in general, this involves rigid objects (such as cars[38]) or objects with a predictable behavior (such as humans[39] or animals[40]). Another difference with the current application is the fact that tracking is traditionally established using sequences of tens to hundreds of images and not only a few. Matched points can be used to identify and track linear structures in sequences of images. Corresponding linear structures are those structures that contain common matched points, as the example shown in Fig. 14.21. Linear structures that do not contain any control points remain unmatched (note that these are likely to be small structures).

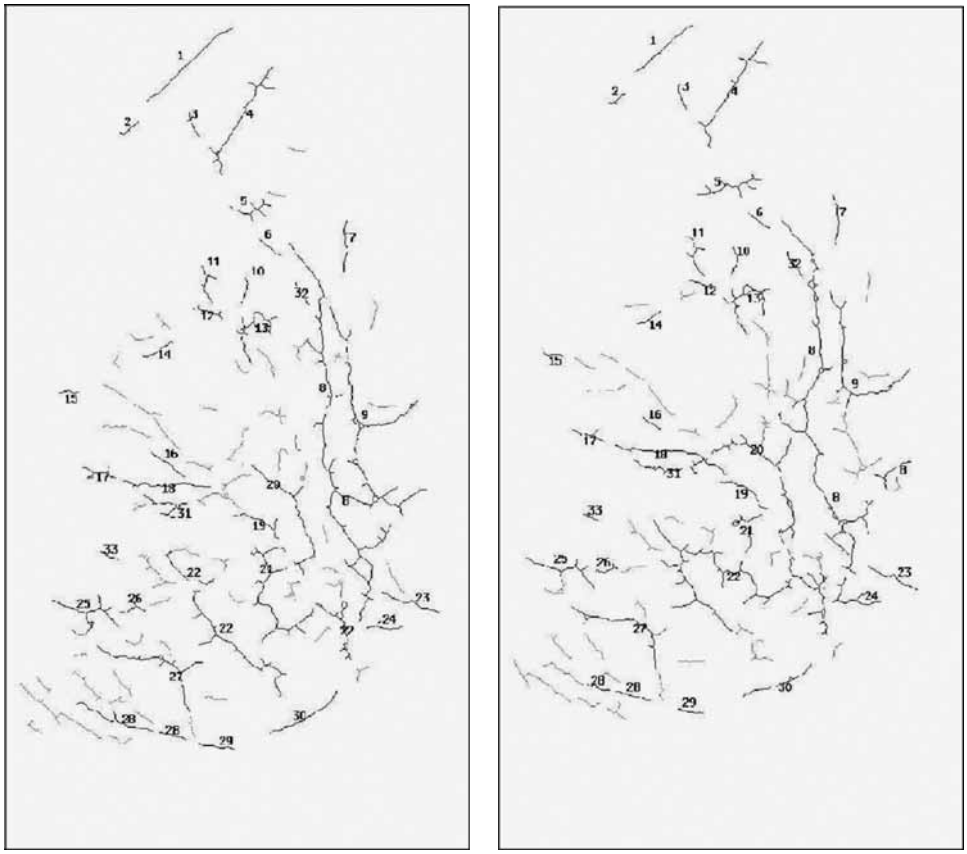

(a) (b)

Figure 14.21 Tracking of linear structures: (a) original and (b) deformed mammograms.

14.6.1 EVALUATION

To demonstrate the proposed tracking method, it is tested using mammographic images. Figure 14.21 shows tracking between a mammogram and a deformed version of itself (the deformation has a local nature and is based on registration between screening rounds), where numbers depict corresponding linear structures. This indicates the local movement of the linear structures. Due to line fragmentation, linear structures in one image may correspond to more than one linear structure in the other. This explains the repeated numbers in Fig. 14.21. It can be seen that major linear structures have been successfully identified and tracked.

Using the example of Fig. 14.21, the robustness of the tracking algorithm was tested in the presence of noise and outliers. Evaluation has been carried out counting the number of matching errors found in the images. It should be noted that a matching error does not mean that both corresponding structures are com-

pletely mismatched, since linear structures are being mathched not only points. Therefore, the number of matching errors and the number of matches are not related.

Figure 14.22(a) shows the number of matching errors found in the images when different amounts of Gaussian noise $N(\mu, \sigma)$ are added to the feature points. At each plotted point in Fig. 14.22(a), noise is affecting all features: position with $N(0, 20)$, orientation with $N(0, \pi/6)$, and width with $N(0, 10)$. It should be noted that noise for each point is added to the previous noise level and the graph presents a linear behavior that denotes the robustness of the method. Another test has been performed to determine the dependence of the method on the presence of outliers. Outliers are defined here as matched points that are not related to major mammographic linear structures; most of the time these are due to noise, image artifacts, or spurious structures. Outliers have been generated using the following method: a number of initially extracted feature points have been randomly removed and replaced by the same number of randomly generated points. Figure 14.22(b) plots the number of matching errors as a function of the percentage of those outliers. Again, the response presents a linear behavior, even with a large percentage of outliers.

14.6.2 RESULTS

This section presents initial tracking results. Figure 14.23 shows the tracking of linear structures in temporal mammograms. It can be seen that tracking results are not as good as in the test image in Fig. 14.21, but major linear structures are still being tracked. It should be noted that the abnormality occurs in an area that does not contain a large number of matched mammographic linear structures.

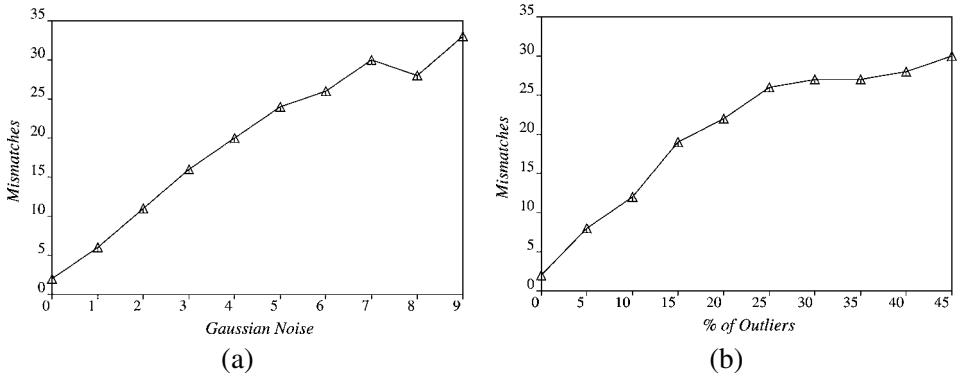

Figure 14.22 Evaluation of the tracking of linear structures: (a) Gaussian noise added to feature points and (b) presence of outliers.

14.7 AUTOMATIC MR CORRESPONDENCE BASED ON LINEAR STRUCTURES

This section extends the registration algorithm described in the previous section to MR (3D) registration. The approach is also based on finding correspondence between internal structures in images given by matching features extracted from salient points.

Registration could be applied to dynamic MR studies, where MR volumes are taken at short intervals after a contrast agent is injected and tissue uptake measured. Misalignment in such cases is generally of small magnitude and of nonlinear nature, both due to involuntary movement (i.e., breathing and heart beat, among others). Figure 14.24 shows an example of a dynamic MR study where pre- and postcontrast volumes are shown.

On the other hand, temporal MR registration could also be performed using volumes obtained at longer intervals, typically periods ranging from months to a

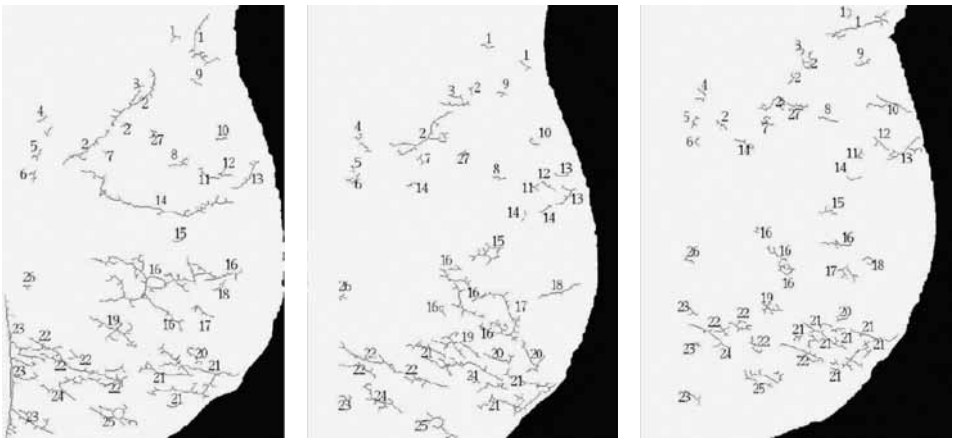

(a) (b) (c)

Figure 14.23 Tracking of linear structures in mammograms from various screening years: (a) 1992; (b) 1995; and (c) 2000.

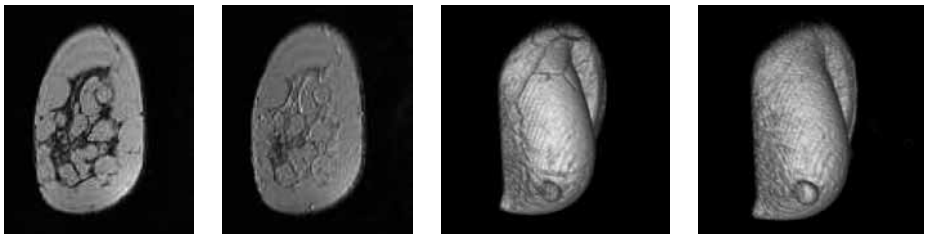

(a) (b) (c) (d)

Figure 14.24 Slices and volume renderings from a dynamic study: (a) and (c) precontrast, and (b) and (d) postcontrast acquisitions.

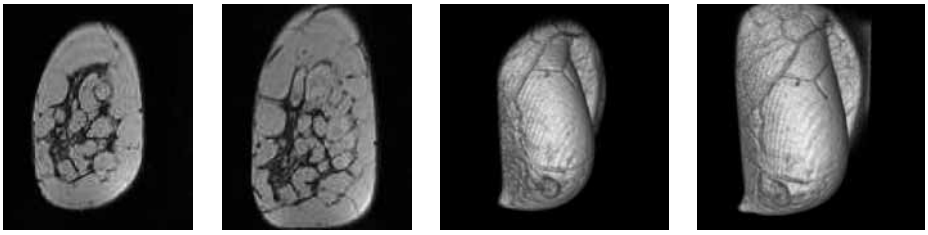

(a) (b) (c) (d)

Figure 14.25 Slices and volume renderings from a temporal study: (a) and (c) February, and (b) and (d) April acquisitions.

year. These temporal series are often used for women to monitor the development of detected abnormalities. In addition, the success of treatment (i.e., chemotherapy) is often evaluated by acquiring MR volumes at shorter intervals (typically days or weeks). As expected, images taken at larger intervals suffer larger misalignments compared to dynamic cases. This is due to the fact that the patient is repositioned for acquisition. This is illustrated in Fig. 14.25, which shows an example of a temporal MR study.

In all registration cases, being able to find correspondence between areas in various volumes would help to detect changes in the breast such as an increasing contrast region or a recently developed suspicious area. In addition, as mentioned before, being able to track regions in images would also help to assess the efficiency (i.e., tumour regression) of an ongoing therapy.

14.7.1 REVIEW

Looking at the existing literature, there are only a limited number of publications addressing the problem of image registration applied to MR images or any other applications with similar implications. This could be explained by the relatively recent need for such methodologies mainly due to the increasing spread of MR in mammography, especially in countries where its use in screening is being investigated [i.e., the magnetic resonance imaging for breast screening (MARIBS) study[41]]. Moreover, approaches published so far limit their application to the registration of dynamic sequences, where deformations are generally less severe. Although dynamic sequences are more common than temporal analysis (where images are more difficult to obtain), it is our aim to investigate a common approach for both registration cases. The developed method should not rely on intensity correlation between images because, as shown in Fig. 14.24, dynamic studies show intensity variations depending on the contrast-agent uptake. Therefore, similarity measures such as mutual information are expected to provide more accurate results.[15,23] About the work published by other authors, one should mention the approach taken by Hayton et al.[13] who applied (2D) registration to pre- and post-contrast MR slices using an optical flow model based on a Bayesian formulation

and maximization of mutual information. Rueckert et al.[12] also proposed a novel registration approach based on mutual information. They described a 3D nonrigid registration algorithm based on a B-spline grid that deformed, maximizing a cost function based on a mutual-information measure and additional smoothness constraints. Although other approaches have been proposed, their applicability is questionable since they either make the assumption of a rigid transformation[42] or linear intensity correlation in dynamic studies.[43]

14.7.2 METHODOLOGY

The correspondence problem is addressed by proposing a methodology that aims to match salient internal structures such as linear structures (i.e., vessels, ducts) and tissue boundaries. This can be regarded as an extension to the third dimension of the approach described in the previous section. As in the 2D case, correspondence is based on matching salient points along the linear structures. Those points happen to be invariant to intensity correlation and nonsevere (realistic) nonlinear deformations. The intensity invariance is due to the use of features from the linear structures instead of intensity information as such. Moreover, when a measure of similarity is used (i.e., in the matching process), mutual information is chosen due to its independence on image intensity. If the assumption of a nonsevere nonlinear transformation holds, the linear structures would present a similar overall structure. Once points have been extracted, matches in MR volumes are found by comparing their local features, such as orientation, width, and position, using the same distance matrix matching approach. Potential matches are assumed to lie in approximately the same volume after a global alignment is carried out based on maximizing a normalized mutual-information measure using a rigid transformation.

A multilevel alignment could also be used here, as in the x-ray case, but due to the small size of the subimages, the mutual-information measure did not return robust results. This is due to the statistical weakness of the intensity distribution induced by interpolation artifacts.[21,44] The use of methods to robustly estimate the probability distribution could be applied (as in Ref. 44), but this will need further investigation. Therefore, a single-level matching approach is used here.

Finally, volumes are aligned using the matched points and a point-based method such as volume, thin-plate, or elastic-body splines. Here, an elastic-body spline (EBS)[17] mapping function is used based on a deformation model of an elastic material that can be regarded as a simple model of breast tissue. EBS was shown to be more appropriate compared to the other mentioned spline functions applied to MR mammographic registration.[17]

14.7.3 EVALUATION AND RESULTS

Initial results are shown using a synthetic registration case. A volume is matched to a deformed version of itself. The deformation is generated by manually corresponding a number of points and applying an EBS transformation to the volume.

The use of EBS for the generation of the deformed volume can be seen as a drawback of this evaluation, but it should be stressed that the experiment is to show that the points found by the developed approach are reliable, and not to evaluate the EBS method.

Results are shown measuring the similarity [using normalized cross-correlation (CC) and mutual information (MI)] between the registered and original volumes. As seen in Table 14.4, an increased value is always obtained when the registration is applied. A maximum is obtained when using the proposed method.

This is also indicated by looking at the registration images in Fig. 14.26, which show difference images (where darker means larger differences) between the registered and the original volumes for a particular slice. It should be noted that there is a large improvement compared to unregistered and even registration using a global rigid transformation. However, it can be seen that some differences are found in the breast outline area. That will be a common characteristic of registration results with the proposed method that is explained by the fact that only internal linear structures are used for the matching process, aiming to provide an accurate registration of those areas. It is our belief that the use of points along the breast boundary in the MR volume would yield more accurate results in such areas, but this extension is not discussed here and is expected to be incorporated in future work.

14.7.3.1 Registration of temporal sequences

Initial results of registration of temporal MR images are presented in this section. Temporal volumes are difficult to obtain. This fact is reflected by the number of

Table 14.4 Evaluation: similarity measures between registered and original volumes.

Registration	CC	MI
No registration	0.819	0.243
Rigid registration	0.822	0.246
Our approach	**0.850**	**0.286**

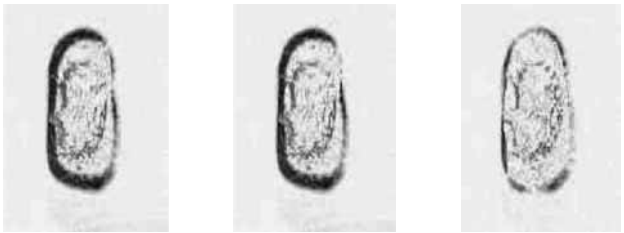

(a) (b) (c)

Figure 14.26 Evaluation: difference image between registered and original volumes for a particular slice, using (a) no registration; (b) rigid registration; and (c) the developed approach.

temporal volumes (only two) available in our database at the time of writing. However, the results obtained are a good example of the additional difficulties involved in this type of registration. Misalignment between images is likely to be large due to the fact that images are acquired at different times, involving patient repositioning and different imaging parameters (i.e., the use of breast compression and different MRI protocols). In general, this misalignment can be described in terms of differences related to pose (therefore involving a rigid transformation) and to local deformation (involving a nonlinear transformation). An example of the former is shown in Figs 14.27(d)–(f), where rigid registration by maximizing the mutual-information measure has been applied to temporal volumes. This process removes pose differences, leaving nonlinear deformations, which are minimized by using the proposed registration approach as shown in Figs 14.27(g)–(i).

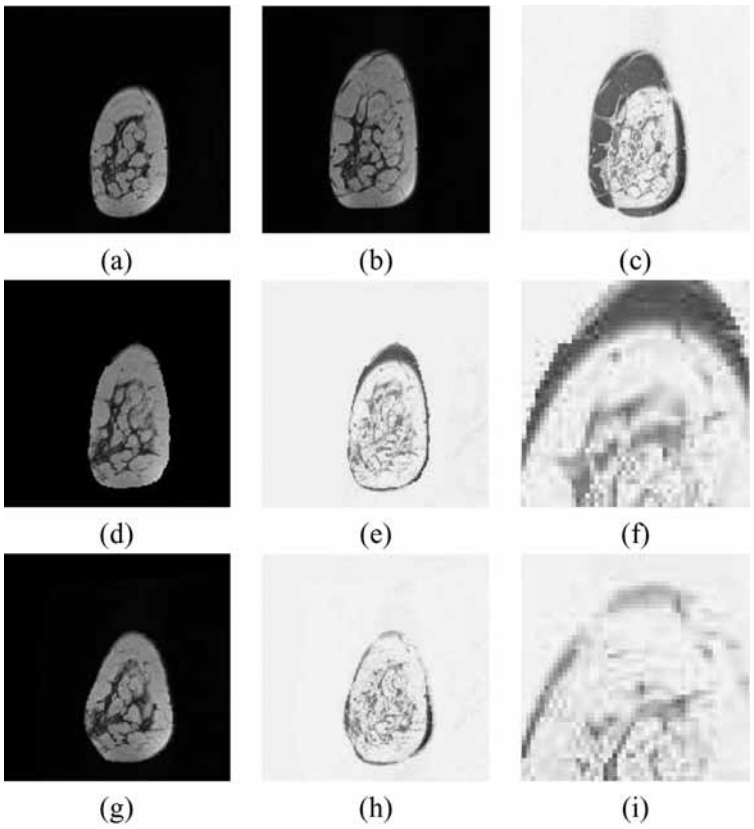

Figure 14.27 Temporal MR registration: recovering pose differences and nonlocal deformation. A slice from the (a) reference and (b) target volumes, and (c) its difference. Registration results (d) using rigid transformation by maximization of mutual information, and (e) and (f) difference between slices. Registration results (g) using the proposed approach, and (h) and (i) difference between slices. Here (f) and (i) show enlarged regions of (e) and (h), respectively.

In temporal studies, the nonlinear magnitude of the deformation could be much larger than the example shown in Fig. 14.27. This fact was experienced for the registration of the second volume, where images present large nonlinear differences that registration was unable to recover. It is blieved that the use of the multilevel approach for the matching would obtain better results since matching at different levels would obtain a better description of the breast deformation, but this is an aspect that will need further development.

Temporal registration results for two cases are also shown in Table 14.5, where similarity measures are computed from volumes using no registration, rigid registration, and the developed approach. Measures agree with the qualitative results shown in the mentioned figures. In all cases, the use of the developed approach yields the best results, even when registration fails (Table 14.5b).

14.7.4 SUMMARY

A novel method to register MR breast images based on correspondence between their internal linear structures has been presented. This was based on the methodology described for the 2D case.

Initial results using synthetic and real data indicate the validity of the developed approach, although further evaluation is needed. Interesting results have been obtained for temporal cases where deformation has been recovered successfully, with the exception of a case of a severe distortion. However, the inclusion of other features (local intensity similarity) along with a multilevel implementation of the point-matching process could improve the robustness of the method, and will be investigated.

Correspondence is only based on matching meaningful anatomical structures found in both images; therefore, in principle, differences (due to the presence of abnormalities or severe structural changes) are not used in the correspondence. This latter aspect can be seen as a drawback of methods such as those in Refs. 12 and 13 which use the whole image (inclusive of any abnormalities when present) to obtain correspondence.

Although the method was applied to mammography, it is believed that the method can be applied to any 3D data that incorporates some sort of structural information (i.e., MR of other body areas, or CT images) since no data-related as-

Table 14.5 Temporal MR registration: similarities between registered and original volumes using no registration, rigid registration, and the developed approach for the two cases.

(a)	CC	MI	(b)	CC	MI
No registration	0.607	0.091	No registration	0.383	0.092
Rigid registration	0.856	0.124	Rigid registration	0.459	0.088
Our approach	**0.884**	**0.147**	Our approach	**0.465**	**0.092**

sumptions have been introduced. This, along with further evaluation using a larger MR breast database, will be the focus of future work.

14.8 CONCLUSIONS

The work presented here describes a novel approach to solve the problem of extracting of reliable features in mammographic images, and establishes correspondence between them in pairs of mammograms.

It has been shown here that features extracted from linear structures can provide a robust automatic approach to the generation of control points for image registration. Local features based on scale, orientation, and position have been used. In addition, it is clear that the use of the multilevel approach provides additional information about breast deformation that helps to improve the robustness of the method.

Initial results based on a temporal and contralateral comparison indicate that the automatic approach is comparable to manual registration. Different applications have been developed based on the same correspondence principles. Automatic registration of normal and abnormal temporal mammograms has shown that it is feasible to develop automatic approaches for the detection of structural abnormalities based on the analysis of the difference image. Although not developed here, classification could be used to provide a diagnosis based on those results. The analysis of abnormal temporal mammograms showed that images presented slight differences in years before the abnormality was diagnosed that could indicate early signs of cancer. Registration in this case could also be used as a training tool to study the same region over time in order to assess any differences. Another application is the development of a framework to track internal linear structures in temporal mammographic images. Initial results show that this could be beneficial to assess structural breast changes due to the development of abnormalities.

Registration and tracking results strongly rely on satisfactory line and feature detection, which is not straightforward to achieve because of different and uncontrollable imaging conditions (breast compression, radiation exposure, and patient movement). However, for the different applications presented, promising results were obtained. Further work could be focused on incorporating additional features from the salient points such as local shape contexts[45] that also make use of intensity information.

In addition, other line-detection methods and image-normalization approaches could be investigated. Linear structures appear to be nonuniformly fragmented over the images. Line-linking algorithms could be applied, but special care has to be taken in choosing the linking criterion due to the complex geometry of the linear structures. Finally, statistical modeling of the tracked abnormal regions over time can also be used to assess the subtle presence of abnormalities in early screenings.

REFERENCES

1. K. Marias, J.M. Brady, R.P. Highnam, S. Parbhoo, and A.M. Seifalian, "Registration and matching of temporal mammograms for detecting abnormalities." *3rd Conference on Medical Image Understanding and Analysis* (1999).
2. M. Sallam and K. Bowyer, "Registration and difference analysis of corresponding mammogram images." *Med. Image Anal.* **3**(2), pp. 103–118 (1999).
3. N. Karssemeijer and G. Te Brake, "Combining single view features and asymmetry for detection of mass lesions." *4th International Workshop on Digital Mammography*, pp. 95–102. Kluwer, Dordrecht (1998).
4. K. Marias, C.P. Behrenbruch, M. Brady, S. Parbhoo, and A. Seifalian, "Multiscale landmark selection for improved registration of temporal mammograms." *5th International Workshop on Digital Mammography*, pp. 580–586, Medical Physics Pub., Madison, WI (2000).
5. S. Kok-Wiles, M. Brady, and R. Highnam, "Comparing mammogram pairs for the detection of lesions." *4th International Workshop on Digital Mammography*, pp. 103–110. Kluwer, Dordrecht (1998).
6. N. Vujovic and D. Brzakovic, "Establishing the correspondence between control point in pairs of mammographic images." *IEEE Trans. Image Process.* **6**(10), pp. 1388–1399 (1997).
7. F.L. Bookstein, "Principal warps: thin-plate splines and the decomposition of deformations." *IEEE Trans. Pattern Anal. Mach. Intell.* **11**(6), pp. 567–585 (1989).
8. M. Bhattacharya and D.D. Majumder, "Registration of CT and MR images of Alzheimer's patient: a shape theoretic approach." *Pattern Recogn. Lett.* **21**, pp. 531–548 (2000).
9. J.B.A. Maintz, P.A. van den Elsen, and M.A. Viergever, "3D multimodality medical image registration using morphological tools." *Image Vision Comput.* **19**, pp. 53–62 (2001).
10. J.B.A. Maintz, P.A. van den Elsen, and M.A. Viergever, "Evaluation of ridge seeking operators for multimodality medical image matching." *IEEE Trans. Pattern Anal. Mach. Intell.* **18**(4), pp. 353–365 (1996).
11. J. Feldmar, N. Ayache, and F. Betting, "3D-2D projective registration of free-form curves and surfaces." *Comput. Vision Image Understanding* **65**(3), pp. 403–424 (1997).
12. D. Rueckert, L.I. Sonoda, C. Hayes, D.L.G. Hill, M.O. Leach, and D.J. Hawkes, "Nonrigid registration using free-form deformations: application to breast MR images." *IEEE Trans. Med. Imaging* **18**(8), pp. 712–721 (1999).
13. P.M. Hayton, M. Brady, S.M. Smith, and N. Moore, "A nonrigid registration algorithm for dynamic breast MR images." *Artificial Intell.* **114**, pp. 125–156 (1999).
14. F. Maes, D. Vandermeulen, and P. Suetens, "Comparative evaluation of multiresolution optimization strategies for multimodality image registration by

maximisation of mutual information." *Med. Image Anal.* **3**(4), pp. 373–386 (1999).
15. W.M. Wells, P. Viola, H. Atsumi, S. Nakajima, and R. Kikinis, "Multi-modal volume registration by maximization of mutual information." *Med. Image Anal.* **1**(1), pp. 35–51 (1996).
16. J.W. Weaver, D.M. Healy, S. Periaswamy, and P.J. Kostelec, "Elastic image registration using correlations." *J. Digital Imaging* **11**(3), pp. 59–65 (1998).
17. M.H. Davis, A. Khotanzad, D.P. Flaming, and S.E. Harms, "A physics-based coordinate transformation for 3-D image matching." *IEEE Trans. Med. Imaging* **16**(3), pp. 317–328 (1997).
18. F. Maes, A. Collignon, D. Vandermeulen, G. Marchal, and P. Suetens, "Multimodality image registration by maximization of mutual information." *IEEE Trans. Med. Imaging* **16**(2), pp. 187–198 (1997).
19. P.A. Viola, "Alignment by maximization of mutual information." Ph.D. thesis, Massachusetts Institute of Technology (1995).
20. S. Ourselin, A. Roche, G. Subsol, and X. Pennec, "Automatic alignment of histological sections." *International Workshop on Biomedical Image Registration*, pp. 1–13 (1999).
21. B. Likar and F. Pernus, "Elastic registration of muscle fiber images." *International Workshop on Biomedical Image Registration*, pp. 24–45 (1999).
22. C.E. Shannon, "A mathematical theory of communication." *Bell Syst. Tech. J.* **27**, pp. 379–423 and 623–656 (1948).
23. F. Bello and A.C.F. Colchester, "Measuring global and local spatial correspondence using information theory." *1st International Conference Medical Image Computing and Computer-Assisted Intervention*, pp. 964–973 (1998).
24. A. Rangarajan, H. Chui, and J.S. Duncan, "Rigid point feature registration using mutual information." *Med. Image Anal.* **3**(4), pp. 425–440 (1999).
25. R. Chandrasekhar, "Systematic segmentation of mammograms." Ph.D. thesis, University of Western Australia (1996).
26. M.Y. Sallam, "Image unwarping and difference analysis: a technique for detecting abnormalities in mammograms." Ph.D. thesis, University of South Florida (1997).
27. R. Chandrasekhar and Y. Attikiouzel, "A simple method for automatically locating the nipple on mammograms." *IEEE Trans. Pattern Anal. Mach. Intell.* **16**(5), pp. 483–494 (1997).
28. N. Karssemeijer, "Automated classification of parenchymal patterns in mammograms." *Phys. Medicine Biol.* **43**, pp. 365–378 (1998).
29. R. Zwiggelaar, S.M. Astley, C.R.M. Boggis, and C.J. Taylor, "Linear structures in mammographic images: Detection and classification." *IEEE Trans. Med. Imaging* **23**(9), pp. 1077–1086 (2004).
30. G. Medioni and R. Nevatia, "Matching images using linear features." *IEEE Trans. Pattern Anal. Mach. Intell.* **6**(6), pp. 675–685 (1984).
31. Y. Chang and J.K. Aggarwal, "Line correspondences from cooperating spatial and temporal grouping processes for a sequence of images." *Comput. Vision Image Understanding* **67**(2), pp. 186–201 (1997).

32. R. Marti, R. Zwiggelaar, and C.M.E. Rubin, "A novel similarity measure to evaluate image correspondence." *Proc. Of International Conference on Pattern Recognition*, pp. 3171–3174 (2000).
33. J. Deschênes and D. Ziou, "Detection of line junctions and line terminations using curvilinear features." *Pattern Recogn. Lett.* **21**, pp. 637–649 (2000).
34. V. Lacroix and M. Acheroy, "Feature extraction using the constrained gradient." *Photogrammetry Remote Sensing* **53**, pp. 85–94 (1998).
35. G. Borgefors, "Hierarchical chamfer matching: A parametric edge matching algorithm." *IEEE Trans. Pattern Anal. Mach. Intell.* **10**(6), pp. 849–865 (1988).
36. P.J. Besl and N.D. McKay, "A method for registration of 3-D shapes." *IEEE Trans. Pattern Anal. Mach. Intell.* **14**(2), pp. 239–256 (1992).
37. T. Drummond and R. Cipolla, "Real-time tracking of complex structures with on-line camera calibration." *10th British Machine Vision Conference*, pp. 574–583 (1999).
38. J.M. Ferryman, S.J. Maybank, and A.D. Worrall, "Vehicle tracking with applications to collision alert." *8th British Machine Vision Conference*, pp. 192–201 (1997).
39. I.A. Kauralova, P.M. Hall, and A.D. Marshall, "A hierarchical model of dynamics for tracking people with a single video camera." *11th British Machine Vision Conference*, pp. 352–361 (2000).
40. N. Sumpter, R.D. Boyle, and R.D. Tillett, "Modelling collective animal behaviour using extended point distribution models." *8th British Machine Vision Conference*, pp. 242–251 (1997).
41. The Institute of Cancer Research, *Magnetic Resonance Imaging for Breast Screening*. http://www.icr.ac.uk/cmagres/maribs/maribs.html (accessed 03/06/02).
42. C.S. Zuo, A. Jiang, B.L. Buff, T.G. Mahon, and T.Z. Wong, "Automatic motion correction for breast MR imaging." *Radiology* **198**(3), pp. 903–906 (1996).
43. H. Fischer, M. Otte, C. Ehritt-Braun, M. Büchert, S. Peschl, and J. Hennig, "Local elastic motion correction in MR-mammography." *International Society of Magnetic Resonance in Medicine*, Vol. 1, p. 725 (1998).
44. J.P.W. Pluim, J.B.A. Maintz, and M.A. Viergever, "Mutual information matching in multiresolution contexts." *International Workshop on Biomedical Image Registration*, pp. 46–60 (1999).
45. S. Belongie, J. Malik, and J. Puzicha, "Shape matching and object recognition using shape contexts." *IEEE Trans. Pattern Anal. Mach. Intell.* **24**(4), pp. 509–522 (2002).